

Joint Stiffness Adjustment of a Pneumatic Driven Exoskeleton

Pavel Venev^a, Dimitar Chakarov^b and Ivanka Veneva^c

Institute of Mechanics, Bulgarian Academy of Sciences, "Acad. G. Bonchev" str., Block 4, Sofia 1113, Bulgaria

Keywords: Exoskeleton, Upper Limb, Transparency, Pneumatic, Cylinders, Stiffness, Torque, Air Pressure, Closed Chambers, Gravity Compensation.

Abstract: The work studies an exoskeleton on the upper limb intended for rehabilitation and training. To meet the requirements of rehabilitation exoskeletons for transparency on the one hand and efficiency on the other, a pneumatic actuation with a wide range of control pressure is offered. The subject of the work is the development of a pneumatic drive that allows simultaneous adjustment of stiffness and torque in the joints of the exoskeleton. For this purpose, pressure in the cylinder chambers both higher and lower than atmospheric is used. The work presents the structure of the exoskeleton and a model of pneumatic actuation in the joints of the exoskeleton. Equations are derived for the torque and joint stiffness resulting from the elasticity of the air in the closed chambers of the pneumatic cylinders. The work proposes one approach to adjust the stiffness at certain joint position. In this position, the joint torque is varied by creating pressure profiles in the two chambers, so the joint stiffness is adjusted in addition to the joint torque. The change in joint torque due to elastic deviations from the set position is also evaluated. An example of compensating gravity loads and providing transparency through pneumatic actuation is shown.

1 INTRODUCTION


An alternative to conventional manual therapy for improving motor function in post-stroke patients is the use of robotic exoskeletons for rehabilitation (Manna, 2018). The rehabilitation exoskeleton must be able to create a large force to support, assist and guide the patient's arm in the early stages of recovery, as well as to follow the human arm without resistance by responding to the movements performed by the patient in the full recovery stage (Jarrasse, 2014).


Therefore, in the control of rehabilitation exoskeletons, two ideal modes can be defined that encompass all therapeutic interventions: 'robot in charge' and 'patient in charge' (Veneman, 2006). In the "robot in charge" mode, it is important that the robot has sufficient force and power to realize the desired motion with relatively high impedance. In the "patient in charge" mode, it is important that the interaction forces between the exoskeleton and the human are low, in other words, the perceived


impedance of the patient must be low. The key feature here is transparency.

In order to provide safety and transparency to the interaction, there are two main approaches to change the mechanical impedance of the structure: active and passive. Electric motors and other active actuators are used to control the impedance of rehabilitation exoskeletons through an active approach. Active impedance control is based on the use of sensors and feedback. Impedance control successfully manages patient-exoskeleton interaction in all modes of therapeutic interventions (Courtois G., 2021).

The passive approach involves a natural and inherently safe actuator. Pneumatic actuation has a natural compliance and allows to achieve inherent safety and transparency in the rehabilitation process in a passive manner (Morales, 2011). Pneumatic actuation also allows impedance control via the active approach. There are different types of pneumatic actuators. The best known are conventional pneumatic cylinders and rotary pneumatic motors. On the one hand, they are characterized by large size,

^a  <https://orcid.org/0000-0001-7809-3540>

^b  <https://orcid.org/0000-0002-2312-5725>

^c  <https://orcid.org/0000-0001-5501-7668>

high weight and rigidity of construction, but on the other hand, when mounted in the fixed base, they provide the advantages of pneumatic actuation.

Pneumatic actuators are usually operated at pressures higher than atmospheric pressure. Recently, some soft pneumatic actuators that are activated by vacuum have been developed (Yang D., 2017). Using the effect of mechanical deformation to generate controlled force, vacuum-actuated mechanisms have been successfully developed and used for soft robotic systems (Matthew A., 2017). Vacuum actuators have many advantages over positive pressure actuators. For example, this type of actuator offers implicitly safe operation as the actuation force is limited by the magnitude of atmospheric pressure (Tawk Ch., 2019), also this leads to improved actuator life and durability.

An upper limb pneumatic powered exoskeleton has been developed for training and rehabilitation assisted by interactions in virtual scenes (Chakarov D., 2019). A study was conducted where the exoskeleton driven by pneumatic cylinders with positive pressure was compared with the case where the exoskeleton was driven by pneumatic cylinders with vacuum pressure (Chakarov D., 2022). This study shows that vacuum pressure drive reduces stiffness and results in high transparency and patient safety. However, low stiffness is associated with poor force response and low efficiency when performing "robot-in-charge" operations. The combination of transparency requirements on the one hand and efficiency requirements on the other can be achieved by pneumatic actuators with a wide range of control pressures.

The subject of this work is the development and investigation of a pneumatic actuation for the exoskeleton that allows simultaneous adjustment of stiffness and torque in the joints of the exoskeleton. The goal of the work is to create an approach to adjust the stiffness of the joint and the torque in the joint by driving the pressures in the chambers both higher and lower than atmospheric pressure.

2 STRUCTURE AND MODEL OF PNEUMATIC ACTUATION IN EXOSKELETON JOINTS

A prototype of a lightweight upper limb exoskeleton has been developed by the authors (Chakarov D., 2022). The mechanical structure of the exoskeleton consists of two arms. Each arm includes pairs of identical rotational joints for the movements of the

clavicle J1, J2, shoulder J3, J4 and elbow J5, J6, as shown in Figure 1a, b). The joints have the following range of movement: J1(15°), J2 (15°), J3(120°), J4 (120 °), J5 (150 °), J6 (135 °). Each arm has a total of 6 degrees of mobility, mimicking the natural movement of the human arm from back to elbow. Each arm of the exoskeleton has six movable segments (1, 2, 3, 4, 5 and 6) made primarily of aluminium alloy. Plastic shells with straps are placed on the segments for attachment to the human limb (Figure 1b). This structure was chosen for designing the arm exoskeleton using uniform universal joints and thus avoid more complex solutions involving circular guide and triaxial joints.

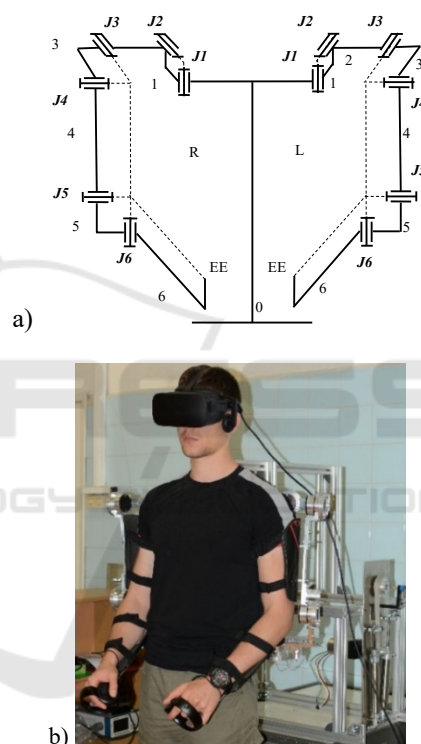


Figure 1: Exoskeleton of the upper limbs: a) structural scheme; b) prototype.

For each joint of the exoskeleton, a drive unit including pneumatic cylinders and cable transmissions was created. The drive unit of each joint is built as a separate device located in the fixed base. A scheme of the drive unit is shown in Figure 2. The base has a bearing wheel 1 with a cable reel R1 mounted on it. Bowden cables T1, T2 are used to connect the reel R1 and a similar reel located in the exoskeleton joint. The radius of reel R₁ is $r = 0.032$ m.

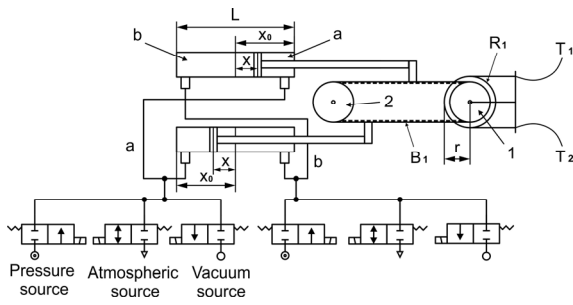


Figure 2: Scheme of the pneumatic drive of exoskeleton joints.

The pneumatic drive unit includes a pair of pneumatic cylinders C1, C2 mounted in the base and a belt transmission as shown in Figure 2. Pneumatic cylinders with a diameter of $D = 0,032$ m are used. The areas on either side of the cylinder piston are $s_1 = 804 \cdot 10^{-6}$ m and $s_2 = 725 \cdot 10^{-6}$ m. The transmission includes a timing belt B1 and an additional wheel 2 for transmitting the motion from the pneumatic cylinders to the wheel 1. The cylinders simultaneously drive opposite sides of the belt B1. The left chamber of one cylinder is connected to the right chamber of the other cylinder by piping, and the other right and left chambers are connected by another piping (Figure 2). The piping of each pair is connected to three parallel valves, one of which supplies pressurized air to the chambers, the other connects the chambers to vacuum pressure, and the third connects the chambers to atmospheric pressure. Pressure sensors are installed on each line.

The work evaluates the interaction between the patient and the exoskeleton in so-called "patient in charge" modes. In this mode, the exoskeleton does not generate active forces. The resisting forces are determined only by the mechanical impedance of the exoskeleton. The resisting force applied to the operator's hand is determined by the inertial, frictional and gravitational forces as well as the elastic forces of the pneumatic actuator.

The joint torque Q_h of the resistive force applied to the operator's arm to overcome the mechanical impedance of the exoskeleton is determined according to equation:

$$Q_h = Q_J + Q_{fr} + Q_g + Q_p \quad (1)$$

Above: Q_J presents the torque created by the motor and the transmissions inertia as well as the exoskeleton inertia; Q_{fr} represents the friction torque which is mainly the result of the friction forces generated in pneumatic actuators and Bowden cables; Q_g is the torque created by the exoskeleton gravity; Q_p is a difference of torques Q_{pa} and Q_{pb} produced

by the forces in the two pneumatic cylinders, represented by the equality

$$Q_p = Q_{pa} - Q_{pb} \quad (2)$$

If one of the chambers of the pneumatic cylinders closes, it generates an elastic force caused by the change in the volume of the enclosed air. The variation of the chamber volume is calculated from the initial piston position X_0 as presented in Figure 2. Assuming that air is an ideal gas undergoing an isothermal process (Czmerk, A., 2017), the rate of change of pressure p and the change of volume V in the closed chamber of the cylinder can be expressed by the equation of the polytrophic process

$$p V = C \quad (3)$$

where C is a constant.

Once in the initial position of the cylinders X_0 (Figure 2), the chamber a of the pneumatic cylinders is closed with a pressure p_a^0 and the volume $V_{(a)}$ of the chamber is represented as a function of the piston area and chamber length, equation (3) takes the form:

$$p_a^0 X_0 (s_1 + s_2) = C_a \quad (4)$$

where s_1 and s_2 are the areas on either sides of the piston and C_a is a constant.

After the arm movements are performed, the piston makes a deviation x from the initial position X_0 (Figure 2) and the pressure p_a in the closed chamber changes. After that, equation (3) should take a new form:

$$p_a (X_0 - x) (s_1 + s_2) = C_a \quad (5)$$

The above equations give the equality for the pressure change p_a as a function of piston deflection x

$$p_a = \frac{p_a^0 X_0}{X_0 - x} \quad (6)$$

The torque of the elastic force in chamber a at deviation of the pistons x from the initial position X_0 is obtained by the equation

$$Q_{pa} = \frac{p_a^0 X_0}{X_0 - x} (s_1 + s_2) r \quad (7)$$

where r is the radius of reel R_1 of Figure 2.

In the same way, when in the initial position of the cylinders X_0 , chamber b is closed with pressure p_b^0 and the piston makes a deviation x from the initial

position X_0 , (Figure 2), equation (3) allows to draw up the following equalities

$$\begin{aligned} p_b^0(L - X_0)(s_1 + s_2) = \\ = p_b(L - X_0 + x)(s_1 + s_2) = C_b \end{aligned} \quad (8)$$

$$p_b = \frac{p_b^0(L - X_0)}{L - X_0 + x} \quad (9)$$

where L is the cylinder length and C_b is a constant.

The equation for the torque of the elastic actuator due to the displacement of the pistons x from the initial position X_0 in chamber b is obtained in a similar way

$$Q_{pb} = \frac{p_b^0(L - X_0)}{L - X_0 + x}(s_1 + s_2)r \quad (10)$$

If either of the chambers a or b of the cylinders is open to the atmosphere, the air in it does not change its pressure and volume, so that the moments generated by the pneumatic forces in the chambers are constant as defined by the equations

$$Q_{pa} = p_{atm}(s_1 + s_2)r \quad (11)$$

$$Q_{pb} = p_{atm}(s_1 + s_2)r \quad (12)$$

In equations (5) - (10) piston deviation x is determined by the deviation q at the joint angle and the radius r of the wheel R_1 as follows

$$x = qr \quad (13)$$

The behavior of closed pneumatic cylinders according to (7) and (10) behaves like a variable compliance spring. The stiffness of the joint driven by pneumatic cylinders can be determined as a derivative of the joint torque (2) about the joint deviation, according to the equality:

$$K = \frac{\partial Q_p}{\partial q} = \frac{\partial Q_{pa}}{\partial x} \frac{\partial x}{\partial q} - \frac{\partial Q_{pb}}{\partial x} \frac{\partial x}{\partial q} = K_a - K_b \quad (14)$$

After differentiation of equations (7) and (10), taking into account (13), the equations for the joint stiffness as a result of the elasticity of the air in chambers a and b are obtained as follows

$$K_a = -\frac{p_a^0 X_0}{(X_0 - x)^2}(s_1 + s_2)r^2 \quad (15)$$

$$K_b = -\frac{p_b^0(L - X_0)}{(L - X_0 + x)^2}(s_1 + s_2)r^2 \quad (16)$$

If one of the chambers is open to the atmosphere, according to (11) (12) and (14) it follows that $Q_{p(a,b)} = const.$ and the joint stiffness in chambers a and b is

$$K_a = 0 \quad (17)$$

$$K_b = 0 \quad (18)$$

3 JOINT STIFFNESS ADJUSTMENT

In this work, the possibility of adjusting the stiffness in a certain joint position is investigated. In this position, the joint torque changes linearly for 10 values, from zero at the first point to one positive value at the last point. For each point, the pressures in the two chambers are changed so that the joint stiffness is adjusted in addition to the joint moment. The joint moment and joint stiffness are evaluated at the piston initial location corresponding to the certain joint position when the deviations from this location are zero ($x=0$). The length of the cylinder and the initial location of the piston are selected respectively $L=0.125$ m and $X_0=0.0625$ m (Figure 2). According to (2), (7), (10), the pressure in the chambers is changed linearly to obtain a linear moment variation.

Three pressure variation profiles are proposed: A. Generation of minimum stiffness by vacuum pressure; B. Variable stiffness generation with vacuum pressure and chamber opening; C. Generation of high stiffness by pressures higher than atmospheric pressure.

A. Generation of minimum stiffness by vacuum pressure.

Vacuum pressure in chamber b of the cylinders is used to generate low stiffness values. Chamber a in this phase is open to the atmosphere $p_a=p_{atm}$. Figure 3 shows the pressure variation in chamber a and in chamber b at which the joint moment Q_p increases linearly. In the first phase, the pressure in chamber b drops smoothly from $p_b=100$ kPa and reaches full vacuum $p_b=0$, and chamber a is open $p_a=p_{atm}$, and generates no stiffness. The joint stiffness is determined by relation (14, 16 and 17) for $x=0$ and the joint moment is determined by relations (2), (10) and (11) for $x=0$.

In the second phase, chamber a closes and the pressure in it increases smoothly, while the pressure in chamber b is kept $p_b = 0$. In this case both chambers are closed, the joint stiffness is determined by equations (14), (15) and (16) for $x=0$ and the joint moment is determined by equations (2), (7) and (10) for $x=0$.

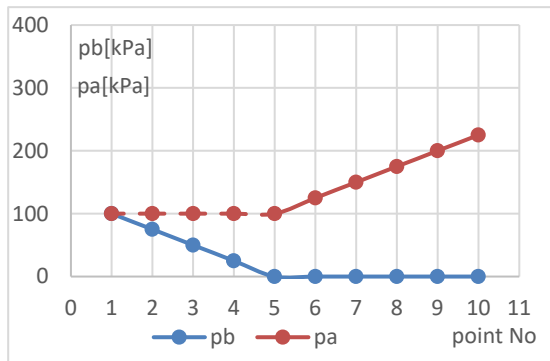


Figure 3: Profile A of pressure variation in chambers a and b of the pneumatic cylinders.

Figure 6 shows the variation of joint moment from 0 to 11.3 Nm as well as the variation of joint stiffness at the ten pressure points. The joint stiffness is minimum in the case when one chamber has full vacuum $p_b = 0$ and the other chamber is open to the atmosphere. The moment in this position is determined by the atmospheric pressure $p_a = 100$ kPa. Further the moment increases as chamber a is closed with higher pressures $p_a > 100$ kPa, at which the stiffness also increases.

B. Variable stiffness generation with vacuum pressure and chamber opening.

Here, a vacuum pressure profile is proposed as a modification of profile A, in which the stiffness is increased by opening the vacuum chamber and using atmospheric pressure.

Figure 4 shows the pressure variation in chamber a and chamber b at which the joint moment Q_p increases linearly. In the first phase, the pressure in chamber b drops smoothly from atmospheric pressure $p_b = 100$ kPa to full vacuum $p_b = 0$, and chamber a is closed in this phase with atmospheric pressure $p_a = 100$ kPa. Since both chambers are closed the joint stiffness is determined by the relation (14), (15) (16) for $x=0$ and the joint moment is determined by equations (2), (7) and (10) for $x=0$.

In the second phase, chamber b is open to the atmosphere, ($p_b = p_{atm}$) and in chamber a, the pressure increases by such values that the moment in the joint increases linearly. In this case, chamber a is closed and chamber b is open and the joint stiffness is determined by relationships (14), (15) and (18). The

moment in the joint is determined by (2), (7) and (12). The piston deviations are zero ($x=0$).

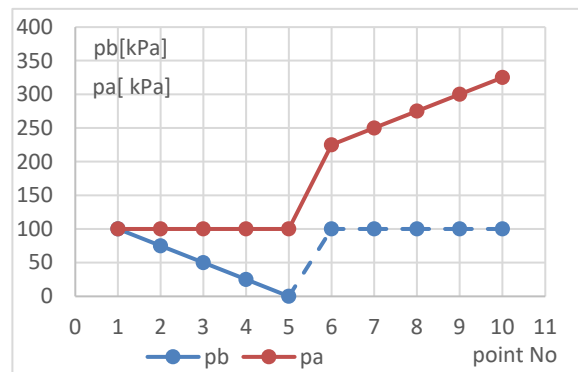


Figure 4: Profile B of pressure variation in chambers a and b of the pneumatic cylinders.

Figure 6 shows the variation of joint moment (2) as well as the variation of joint stiffness (14). The joint stiffness changes in a similar way as in profile A, but at higher values. In contrast to the previous case, the increase in stiffness is achieved by chamber a being closed at a pressure equal to atmospheric in the first phase, and chamber b being opened to atmosphere in the second phase. Switching between the two stiffness values is easily achieved by closing and opening to atmosphere the chambers of the cylinders.

C. Generation of high stiffness by pressures higher than atmospheric pressure.

To generate high stiffness, different profiles can be created at pressures higher than atmospheric pressure and the chambers closed. Thus, it is possible to achieve the desired joint moment and high stiffness. Figure 5 shows a variation of pressures in chamber a and chamber b in which the joint moment (2) increases linearly and the pressure profile is similar to that of cases A and B, but at higher values. In the first phase, chamber a is closed with pressure $p_a = 200$ kPa, and the pressure in chamber b drops smoothly from $p_b = 200$ kPa to $p_b = p_{atm}$. Since both chambers are closed, the moment is determined by (2),(7), and(10) and the joint stiffness is determined by the relation (14),(15), and (16). The piston deviations are zero ($x=0$).

In the second phase, chamber b is closed with pressure $p_b = 200$ kPa, and the pressure in chamber a increases by such values that the moment in the joint increases linearly. Here both chambers are closed, the joint moment and joint stiffness are determined by the same relationships.

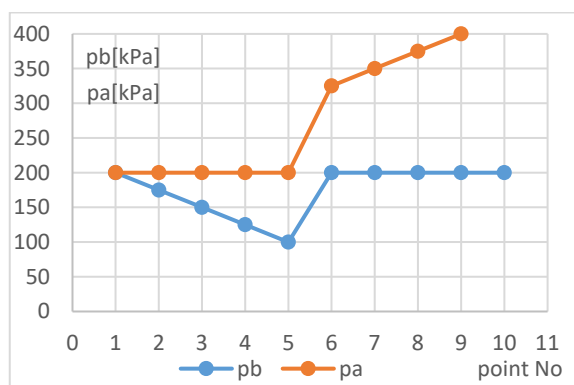


Figure 5: Profile C of pressure variation in chambers a and b of the pneumatic cylinders.

Figure 6 shows the variation of joint moment (2) as well as the variation of joint stiffness (14).

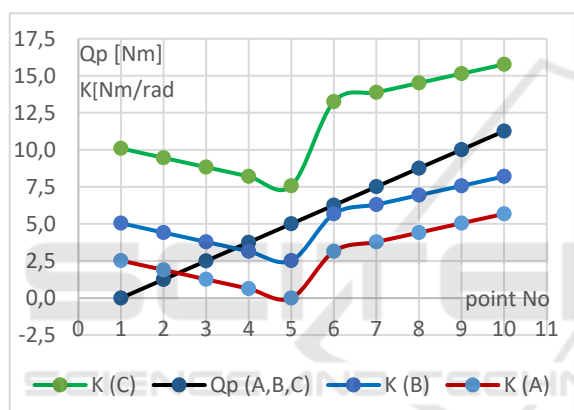


Figure 6: Variation in joint torque and joint stiffness for the three pressure profiles A, B and C.

The joint stiffness profile is similar to the previous cases, but the stiffness values are higher. Of course it is possible to generate stiffness with other modification profiles. A characteristic of the proposed profiles A, B and C is that a minimum stiffness is generated not at zero value but at an average value of the joint moment (5Nm for the considered case). It can be equal to an average value of the joint moment created by static loads on the exoskeleton for the position under consideration. Transparency in this position will be maximized. At any other time in the joint, the stiffness will be higher.

4 JOINT TORQUE ASSESSMENT

When the patient deviates the exoskeleton from the initial position in which any of the cylinder chambers is closed, resistive forces arise as a result of the

elasticity of the closed gas. When both chambers are closed the moment from the elastic forces is determined from equations (2), (7) and (10) as a function of the deviation from the initial position x . For a deviation $x = [-0.014; 0.014]$ m which corresponds according to (13) to a deviation in the joint angle $q = [-0.436; 0.436]$ rad, the variation of the joint moment is shown on Figure 7. The figure shows the variation of the moment in the joint from initial values of 0, 5 and 10 Nm (points 1, 5 and 9 in the graph of Figure 6) at three stiffness values corresponding to the three pressure profiles A, B and C in the graph of Figure 6. Profile A shows the smallest moment variations at all three points.

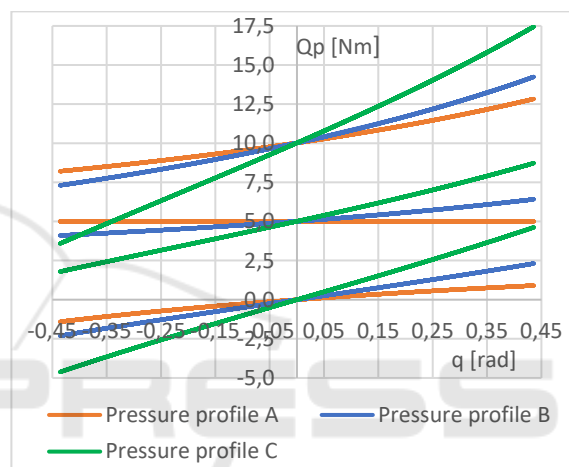


Figure 7: Variation of the joint torque Q_p from initial values of 0, 5 and 10 Nm, corresponding to the three pressure profiles A, B and C.

In the "patient in charge" mode, when the patient performs independent movements, the exoskeleton should provide transparency. For this purpose, the resistive forces due to the mechanical impedance of the exoskeleton must be compensated. In low dynamic mode, only resistance of gravity and stiffness can be taken into account. Then torque (1) of forces applied to the patient's hand is sum of moments of gravity forces and compensatory forces of the pneumatic drive

$$Q_h = Q_g + Q_p \tag{19}$$

In order to achieve transparency, compensatory forces with minimum stiffness must be generated. To compensate for gravity loads, it is appropriate to use the moment from the pneumatic drive achieved at pressures generating the lowest stiffness. Thus, with profile A (Figure 6), the lowest stiffness value is achieved at 5 Nm. Figure 8 shows the variation of the moment from the pneumatic drive at an initial value

of 5 Nm and the pressures in the chambers corresponding to profile A. The figure shows the variation of the gravitational moment in the position of the joint with deviations $q = [0.436; 0.436]$ rad. The resultant moment at the joint according to (19) is also shown in the graph. With small deviations, it oscillates around a zero value, ensuring transparency of the interaction with the patient. Compensating for larger or smaller gravity moments with this pressure profile also results in low resistive forces.

In the 'robot in charge' mode, when the exoskeleton has to implement not only compensation but also the desired movement, it is appropriate to apply a pressure profile similar to the proposed profile C. Figure 9 shows a case when with a torque in the joint of 5 Nm and pressure profile C, the same gravity loads are compensated. Transparency here is lower. Deviations from the set position lead to resistance with significant torque deviations.

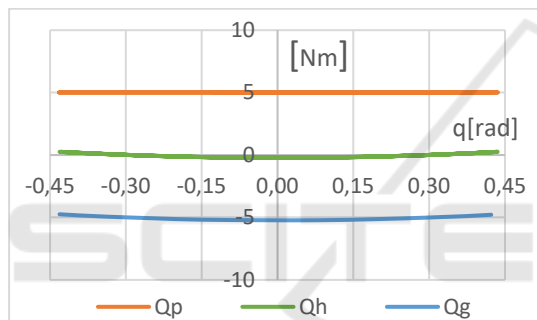


Figure 8: Joint torques deviations after gravity compensation with pressures in the chambers corresponding to profile A.

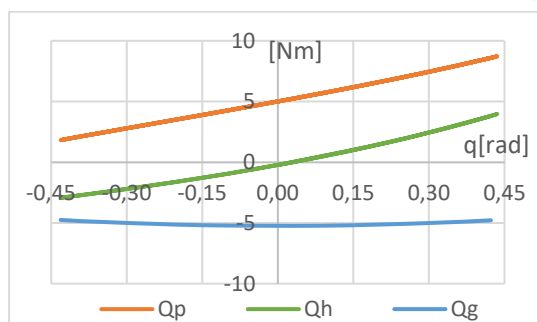


Figure 9: Joint torques deviations after gravity compensation with pressures in the chambers corresponding to profile: C.

5 CONCLUSIONS

The work studies an exoskeleton on the upper limb intended for rehabilitation and training. A pneumatic

drive with a wide range of control pressure is available to meet the requirements of rehabilitation exoskeletons for transparency on the one hand and efficiency on the other. Cylinder chamber pressures both higher and lower than atmospheric are used. The development of a pneumatic drive that allows simultaneous adjustment of stiffness and torque in the joints of the exoskeleton is included in the work. The work presents the structure of the exoskeleton and a model of pneumatic actuation in the joints of the exoskeleton. Equations are derived for the torque and joint stiffness resulting from the elasticity of the air in the closed chambers of the pneumatic cylinders. In the work, an approach for adjusting the stiffness at a certain position of the joint is proposed. In this position, the joint torque is varied by creating pressure profiles in the two chambers, so that the joint stiffness is adjusted in addition to the joint torque. A characteristic of the proposed profiles is that the minimum stiffness is generated not at zero value, but at an average value of the joint torque. To compensate the gravity loads by the pneumatic drive in a certain position, it is appropriate to use the moment corresponding to the lowest stiffness. Then transparency in this position will be best. An example of compensation for gravity when providing transparency through pneumatic activation is shown in the work.

ACKNOWLEDGEMENTS

This research was supported by the Operational Program "Science and education for smart growth" through the project "MIRACle", № BG05M2OP001-1.002-0011 to which the authors would like to express their deepest gratitude.

REFERENCES

- Manna S. K., Dubey V. N., (2018). Comparative study of actuation systems for portable upper limb exoskeletons, *Medical Engineering and Physics*, 60, 1–13.
- Jarrasse, N., T. Proietti, et al., (2014). Robotic Exoskeletons: A Perspective for the Rehabilitation of Arm Coordination in Stroke Patients, *Frontiers in Human Neuroscience*, Vol.8, Art.947, 1-13.
- Veneman, J.F., R. Ekkelenkamp, et al., (2006). A series elastic- and bowden-cable-based actuation for use as torque actuator in exoskeleton-type robots, *The Int. Journ. of Rob. Research*, vol. 25(3), 261-281.
- Courtois G., Chevrie J., Dequidt A., Bonnet X. and Pudlo P. (2021). Design of a Rehabilitation Exoskeleton with Impedance Control: First Experiments. *Proc. of the*

- 18th Int. Conf. on Informatics in Control, Automation and Robotics – ICINCO 2021*, 469-476.
- Morales R., et al., (2011). Pneumatic robotic systems for upper limb rehabilitation, *Med. Biol. Eng. Comput.* 49, 1145–1156.
- Yang D., M. S. Verma, E. Lossner, D. Stothers, G. M. Whitesides, (2017). Negative-pressure soft linear actuator with a mechanical advantage. *Adv. Mater. Technol.*, vol.2, issue 1, 1600164, 1-6.
- Matthew A., Robertson and Jamie Paik, (2017). New soft robots really suck: Vacuum-powered systems empower diverse capabilities. *Science Robotics*, vol. 2, Issue 9, doi: 10.1126/scirobotics.aan6357, 1-27.
- Tawk, C., Spinks, G. M., in het Panhuis, M. & Alici, G. (2019). 3D Printable Linear Soft Vacuum Actuators: Their Modeling, Performance Quantification and Application in Soft Robotic Systems. *IEEE/ASME Transactions on Mechatronics*, 24 (5), 2118-2129.
- Chakarov D., Veneva I., Tsveov M., Mitrouchev P., Venev P. (2019), Design of a Two Arms Exoskeleton as Haptic Device for Virtual Reality Applications, *Lecture Notes in Mech. Eng., Springer Nature*, Chapter 25, 252-262.
- Chakarov, D., Veneva, I., Venev, P. (2022). Comparative Study of a Vacuum Powered Upper Limb Exoskeleton, Pros. of the 19 th Int. Conf. on Informatics in Control, Automation and Robotics, *ICINCO 2022*, 403-410.
- Czmerk, A., A. Bojtos, (2017). Stiffness investigation of pneumatic cylinders, *59th Ilmenau Scientific Colloquium, Technische Universität Ilmenau*, 11 – 15 September, 2017, URN: urn:nbn:de:gbv:ilm1-2017iwk-148:6, 1-7.

